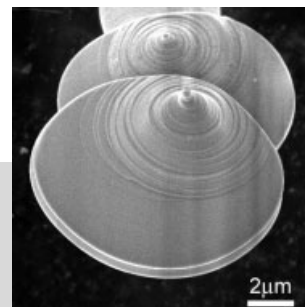


# Nanobelts, Nanowires, and Nanodiskettes of Semiconducting Oxides—From Materials to Nanodevices\*\*

By Zhong Lin Wang\*

*Novel nanostructures of semiconducting oxides are reviewed here. It is shown that nanobelts, nanowires, and nanodiskettes of materials such as zinc oxide, gallium oxide, silica, and tin oxide can be fabricated using a vapor-phase evaporation method. Two applications of these materials—in field effect transistors and as gas sensors—are highlighted.*



## 1. Introduction

Semiconducting oxides are fundamental to the development of smart and functional materials, devices, and systems. The oxides have two unique structural features: mixed cation valences and an adjustable oxygen deficiency, which are the bases for creating and tuning many novel materials' properties, from electric, chemical, and optical to magnetic.<sup>[1]</sup> The synthesis of nanostructures of functional oxides, with a controlled structure and morphology, is critical for scientific and technological applications. Using a novel technique, we have recently synthesized nanobelts,<sup>[2]</sup> nanowires,<sup>[3]</sup> and nanodiskettes of semiconducting oxides. The nanobelts have a ribbon shape with a rectangular cross section and are free from dislocations. Utilizing the high surface area of nanobelt structures, nanoscale devices, such as field effect transistors and gas sensors, have been fabricated, and they have been found to exhibit a superior performance. This paper reviews our progress in the synthesis, characterization, and device applications of these semiconducting oxide nanostructures.

## 2. Vapor-Phase Evaporation Synthesis of Oxide Nanostructures

Vapor-phase evaporation represents the simplest method for the synthesis of one-dimensional oxide nanostructures. By

[\*] Prof. Z. L. Wang  
School of Materials Science and Engineering  
Georgia Institute of Technology  
Atlanta, GA 30332-0245 (USA)  
E-mail: zhong.wang@mse.gatech.edu

[\*\*] Thanks go to Drs. Zhengwei Pan, Zurong Dai, Phedon Avouris, G. Sberveglieri, E. Comini, and J. L. Gole for their contributions, and Mr. Michael Arnold, Chris Ma, Will Hughes, and Ms. Yolande Berta for the work reviewed in this article.

using this method, various kinds of one-dimensional oxide nanostructures, such as nanowires of ZnO,<sup>[4–6]</sup> In<sub>2</sub>O<sub>3</sub>,<sup>[7]</sup> SiO<sub>2</sub>,<sup>[8–10]</sup> Ga<sub>2</sub>O<sub>3</sub>,<sup>[11–13]</sup> and GeO<sub>2</sub>,<sup>[14]</sup> nanobelts of ZnO, SnO<sub>2</sub>, Ga<sub>2</sub>O<sub>3</sub>, In<sub>2</sub>O<sub>3</sub>, CdO, and PbO<sub>2</sub>,<sup>[2,15,16]</sup> and nanorods of MgO<sup>[17]</sup> have been successfully generated. The synthesis is based on the vaporization of oxide powders at a high-temperature zone, and their subsequent deposition in the downstream direction, which results in the formation of specific nanostructures at specific temperature zones. The desired source oxide material (usually in the form of a powder) is placed at the center of an alumina or quartz tube that is inserted into a horizontal tube furnace, where the temperature, pressure, and evaporation time are controlled. Before evaporation, the reaction chamber is evacuated to  $\sim 1\text{--}3 \times 10^{-3}$  torr by a mechanical rotary pump. At the reaction temperature, the source material is heated and evaporated, and the vapor is transported by a carrier gas (such as argon) to the downstream end of the tube, and is finally deposited onto either a growth substrate or the inner wall of the alumina or quartz tube. In our experiments, the products were deposited on an alumina plate placed at the downstream end of the alumina tube.

## 3. Oxide Nanobelts and Nanosheets

The transmission electron microscopy (TEM) images in Figure 1 show the typical shapes of oxide nanobelts of several materials made by vapor phase evaporation.<sup>[2]</sup> Each nanobelt has a uniform width along its entire length, and the typical widths of the nanobelts are in the range of 50 to 300 nm. No particle was observed at the ends of the nanobelts, thus, the vapor–liquid–solid (VLS) process may not be the dominant growth mechanism. The ripple-like contrast that appears in the TEM image is due to strain that resulted from the belt bending. Cross-sectional TEM images show that the nanobelts

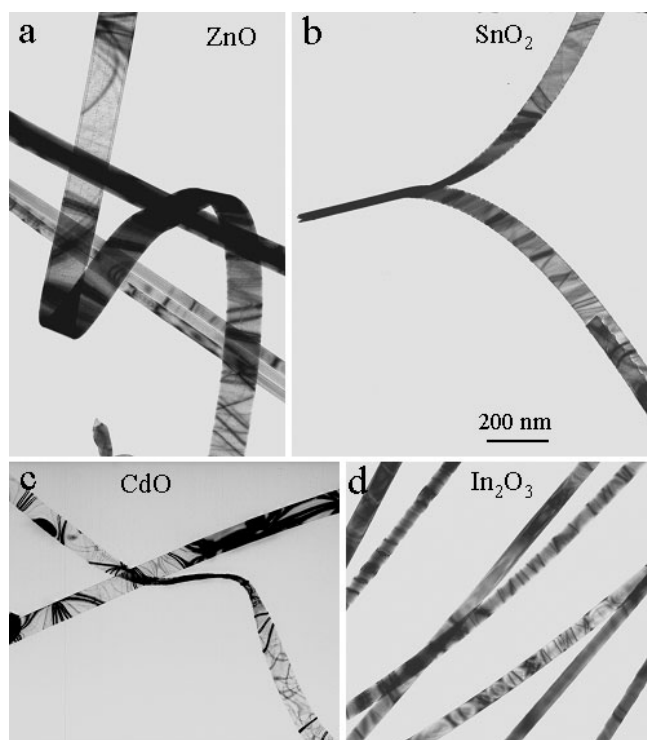


Fig. 1. TEM images of nanobelts of four different oxide materials synthesized by the vapor–solid process, showing their ribbon shape. The raw material used for the synthesis of the nanobelts was the corresponding chemical powder. The scale bar is the same for all four images.

have a rectangular-like cross section, with typical thicknesses in the range of 10 to 50 nm and width-to-thickness ratios of ~3–10. The nanobelts grew along specific directions, and their surfaces are defined by specific crystallographic planes. This means that the nanobelts are structurally and morphologically controlled, and will have controlled properties. Table 1 summarizes the structural characteristics of the nanobelts grown in our laboratory. It seems that the nanobelt morphology is a unique and common structural characteristic for the family of semiconducting oxides.

The growth of a nanobelt is related to two factors. The surface energy determines the preferential surfaces that will grow, whereas the growth kinetics determine the final structure. CdO, for example, has a cubic structure that should have equivalent growth rates along  $\langle 100 \rangle$ , because the  $\{100\}$  surfaces have the lowest surface energy. But the formation of a

Table 1. Semiconductive oxide nanobelts and their growth directions and surface planes.

Nanobelts	Crystal structure	Growth direction/plane	Top surfaces	Side surfaces
ZnO	Wurtzite	[0001]	$\pm(2\bar{1}\bar{1}0)$	$\pm(0\bar{1}\bar{1}0)$
ZnO	Wurtzite	[01 $\bar{1}$ 0]	$\pm(2\bar{1}\bar{1}0)$	$\pm(0001)$
Ga <sub>2</sub> O <sub>3</sub>	Monoclinic	(010)	$\pm(100)$	$\pm(10\bar{1})$
Ga <sub>2</sub> O <sub>3</sub>	Monoclinic	(001)	$\pm(100)$	$\pm(010)$
SnO <sub>2</sub>	Rutile	[101]	$\pm(10\bar{1})$	$\pm(010)$
In <sub>2</sub> O <sub>3</sub>	C-Rare earth	[001]	$\pm(100)$	$\pm(010)$
CdO	NaCl	[001]	$\pm(100)$	$\pm(010)$
PbO <sub>2</sub>	Rutile	[010]	(201)	$\pm(10\bar{1})$

nanobelt structure with fast growth along [100] is a surprise. Figure 2a shows the nanosheet structure of CdO, which was formed by fast growth along [100] and [010], whereas growth along [001] is suppressed, resulting in the formation of a thin

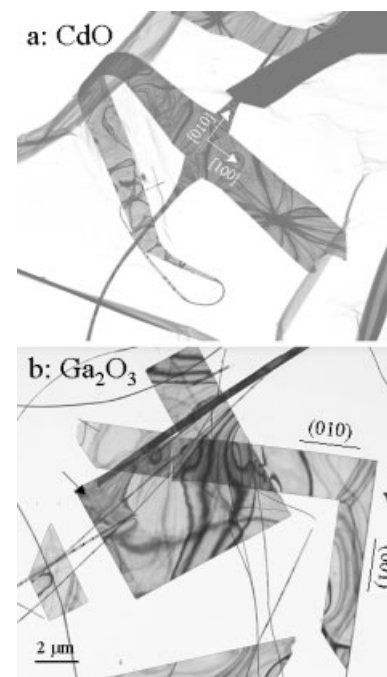


Fig. 2. TEM images showing the nanosheet structures of CdO (a) and Ga<sub>2</sub>O<sub>3</sub> (b) synthesized by the vapor–solid process. The CdO and Ga<sub>2</sub>O<sub>3</sub> nanosheets were made by evaporating CdO and Ga<sub>2</sub>O<sub>3</sub> powder, respectively, using the experimental apparatus employed for nanobelt synthesis. The scale bar is the same for the two images (as displayed in (b)).

sheet type of structure. A similar structure was observed for Ga<sub>2</sub>O<sub>3</sub> (Fig. 2b). The formation of these structures is apparently associated with the growth kinetics.

The next question is “how do the one-dimensional nanostructures form?”, or “what is the growth mechanism of the one-dimensional oxide nanostructures?”. Depending on the presence or absence of metal catalysts in the synthesis processes, two growth mechanisms, i.e., VLS and vapor–solid (VS) mechanisms, have been adopted to account for the growth of the one-dimensional oxide nanostructures. In the VLS process,<sup>[18]</sup> a liquid alloy droplet composed of a metal catalyst component (such as gold, iron, etc.) and a nanowire component is first formed under the reaction conditions. The liquid droplet serves as a preferential site for the adsorption of gas-phase reactant and, when supersaturated, as the nucleation site for crystallization. Nanowire growth begins after the liquid becomes supersaturated in reactant materials and continues for as long as the catalyst alloy remains in a liquid state and the reactant is available. During growth, the catalyst droplet directs the nanowire’s growth direction and defines the diameter of the nanowire.

Unlike the well-developed VLS process, the detail of the VS process, for example, how atoms or other building blocks can be rationally assembled into one-dimensional nanostruc-

tures with wire-like or belt-like morphologies, is still not fully understood. This process is believed to be dominated by the direct vaporization of the solid at a higher temperature zone, with deposition occurring at a lower temperature region. This process appears to be most relevant to the growth of oxide nanobelts.

The formation of long, uniform nanobelts may be described as follows. The solid raw materials are sublimed at high temperature, and the molecular species generated are believed to have the basic structural configuration, such as Zn–O. When the molecules land on the substrate surface, the cation–anion coordinated configuration is preserved to balance the charge for ionically bonded structures. Thus, the crystalline structure is formed. The surfaces that have lower energy tend to grow larger, and they will remain flat even without atom steps at the growth temperature, typically 1000 °C. The low energy surfaces determine the enclosure surfaces of the nanobelt. As a result, no incoming molecules will remain on the flat, low energy surfaces and they tend to diffuse towards the rougher surfaces, which are the growth front, leading to fast growth along this direction and forming the nanobelts. The key question here is “what determines the base size of the nanobelt at the commencement of growth?” More studies are required to answer this question.

#### 4. Networks and Diskettes of Tin Oxide

Tin oxide has been found to exhibit nanostructures of belts/ribbons, wires, networks, and tubes. In addition to the normal rutile structured SnO<sub>2</sub>, we have recently formed an orthorhombic superlattice-like structure.<sup>[3]</sup> The orthorhombic structure can form a thin nanowire, co-exist with the normal rutile structured SnO<sub>2</sub> in a sandwiched nanoribbon, or occur in the form of nanotubes. This result is distinct from that for bulk SnO<sub>2</sub> where pressures in excess of 150 kbar are required to form the orthorhombic form. SnO network and junction structures have also been synthesized:<sup>[19]</sup> they are formed by a fast two-dimensional growth along [100] and [010], while growth along [001] is suppressed.

Most recently, a novel structural form of tin oxide diskette was reported.<sup>[20]</sup> The tin oxide diskettes were synthesized by evaporating either SnO or SnO<sub>2</sub> powders at elevated temperatures (Fig. 3). Regardless of whether the source material was SnO or SnO<sub>2</sub>, the same type of SnO diskette was formed at the lower temperature region of 200–400 °C, indicating that the growth was dominated by the same precursor. Two types of diskette morphologies have been observed, the solid-wheel shape with a drop center rim (type I), and the diskette with a conical peak and spiral steps (type II). Electron microscopy and X-ray diffraction show that the as-synthesized diskettes are a tetragonal SnO structure (*P4/nmm*), with their flat surfaces being (001). For the case of SnO as the source material, the formation of SnO diskettes was within our expectations. When SnO<sub>2</sub> is used as the source material, we propose that the formation of SnO diskettes results from a decomposition

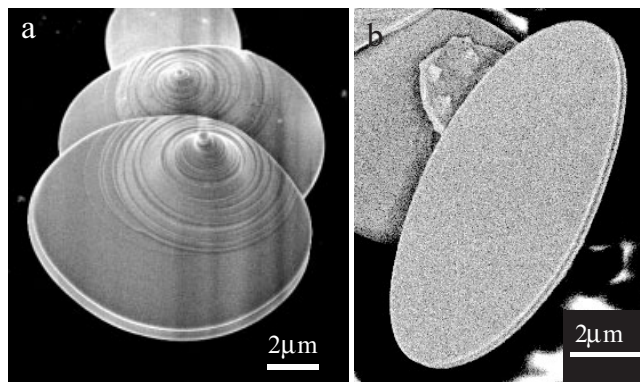


Fig. 3. SEM images of SnO diskettes formed at a lower temperature region of the furnace. The raw materials were either SnO or SnO<sub>2</sub>, and the local substrate temperature was 200–400 °C.

process of SnO<sub>2</sub> → SnO + 1/2 O<sub>2</sub> at high temperature. Since the growth of diskettes occurred in the lower temperature region of 200–400 °C, we propose that the growth of the SnO diskettes resulted from a solidification process.

#### 5. Silica Nanowires

The growth of aligned nanowires is critical for practical applications. A general approach uses nanoparticle-guided growth through the VLS growth process, in which one particle nucleates one nanowire and the size of the particle determines the diameter of the nanowire. Recently, however, we have shown that large (5 to 50 μm diameter), low melting point gallium droplets can be used as an effective catalyst for the large-scale growth of highly aligned, closely packed silica nanowire bunches (Figs. 4a,b).<sup>[21]</sup> The silica nanowires tend to grow batch by batch. For each batch, numerous nanowires simultaneously nucleate, grow at nearly the same rate and direction, and simultaneously stop growing. Tubes with walls composed of highly aligned silica nanowires with diameters of 15 to 30 μm and lengths of 10 to 40 μm were obtained (Fig. 4b). A most amazing phenomenon that we observed was the self-splitting of the silica nanowire, as shown in Fig. 4c: this has not previously been observed in crystalline nanowires.

To offer a simple interpretation of the formation of wire splitting, we first examine the five Zachariasens' rules for oxide glass formation:<sup>[22]</sup> i) oxide glass networks are composed of oxygen polyhedra; ii) the coordination number of each oxygen atom is 2; iii) the coordination number of each metal atom is 3 or 4; iv) oxygen polyhedra share corners, not edges or faces; and v) each polyhedron must share at least three corners. The polyhedron for silica is (SiO<sub>4</sub>)<sup>4-</sup>, which is a tetrahedron. The glass is formed by sharing corners of the tetrahedra, but without translation or orientation symmetry (Fig. 4d). We take tetrahedron B as an example, which has four corners to share. If this tetrahedron is on the surface of the nanowire, another tetrahedron C' can be linked to B via corner sharing, and continuous growth along C' and D' leads to the formation

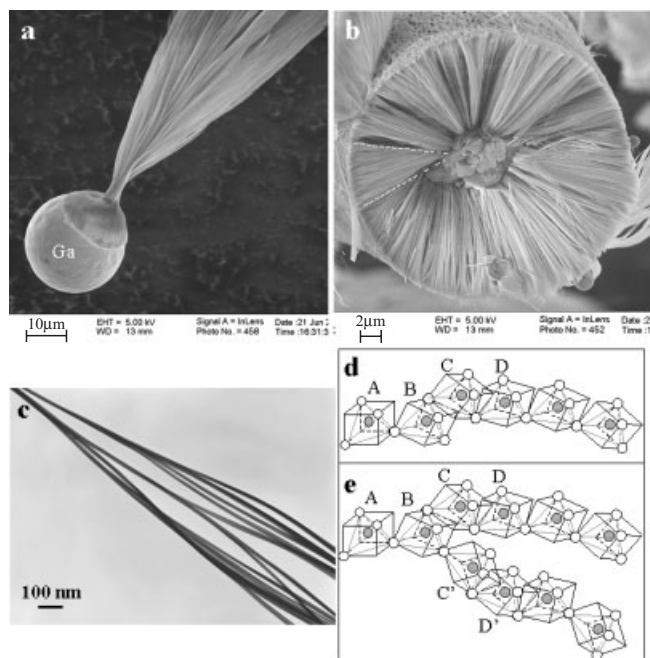


Fig. 4. a,b) SEM images of aligned silica nanowires synthesized by evaporating GaN in the presence of a silicon substrate. The gallium droplet served as the catalyst that led to the nucleation and growth of uniform silica nanowires with diameters of  $\sim 100$  nm. c) The silica nanowires have the characteristic of self-splitting, resulting in thicker bundles as the growth proceeds. d,e) Interpretation of the self-splitting process of the silica glass structure. See text for details.

of another nanowire. The splitting of the nanowire may offer a new approach at the nanoscale level to splitting or converging optical signals using silica nanowires.

## 6. Field-Effect Transistors and Nanosensors Based on Individual Oxide Nanobelts

The structurally and morphologically controlled semiconducting oxide nanobelts are ideal entities for fabricating functional devices. Figure 5a shows a field effect transistor (FET) fabricated using a single ZnO nanobelt,<sup>[23]</sup> and its design principle is given in Figure 5b. By controlling the backgate voltage, switching ratios as large as six orders of magnitude, a conductivity as high as  $10$  ( $\Omega \text{ cm}$ )<sup>-1</sup>, and a mobility as large as  $35 \text{ cm}^2/\text{Vs}$  have been observed. SnO<sub>2</sub> nanobelts can be doped by annealing in reduced oxygen environments, increasing conductivity and drastically decreasing the gate threshold voltage, indicating the feasibility of tuning device characteristics by controlling oxygen vacancies. It has been shown that the FET is very sensitive to UV illumination, and, in turn, the device can be controlled by UV illumination. In ZnO nanobelts, which have a direct bandgap in the UV, two processes have been observed to contribute to photoconductivity. The first process is due to the photogeneration of electron-hole pairs. The second process is most likely due to the desorption of oxygen from the ZnO surface under UV exposure.

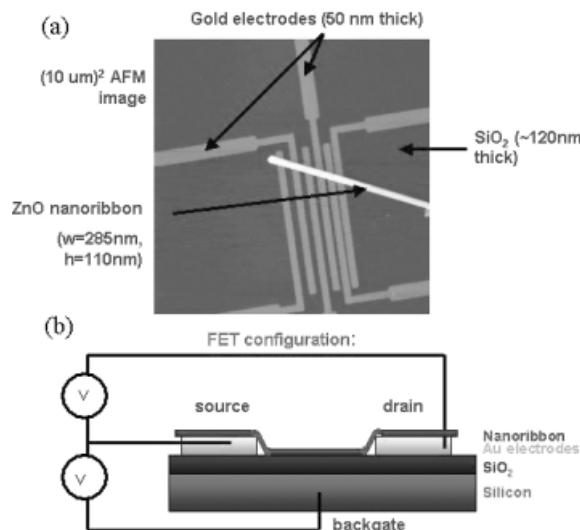


Fig. 5. a) E-beam lithography fabricated field-effect transistor (FET) using a single ZnO nanobelt. b) The working principle of the FET device.

Gas sensors have been fabricated using the single-crystalline SnO<sub>2</sub> nanobelts based on two electrodes contact.<sup>[24]</sup> The conductance of the nanobelt is affected by the surface adsorbed molecules, resulting in a change in the electric current. Electrical characterization showed that the contacts were ohmic and that the nanobelts were sensitive to environmental pollutants such as CO and NO<sub>2</sub>, as well as to ethanol—useful for breath analyzers and food control applications. The sensor response, defined as the relative variation in conductance due to the introduction of the gas, is  $\Delta G/G = 200\%$  for 250 ppm of ethanol and  $\Delta G/G = 3000\%$  for 0.5 ppm nitrogen dioxide at  $200^\circ\text{C}$  (Fig. 6). The sensor displays selectivity between ethanol and NO<sub>2</sub>. These results demonstrate the potential of fabricating nanosize sensors using the integrity of a single nanobelt with a sensitivity at the level of a few parts per billion.

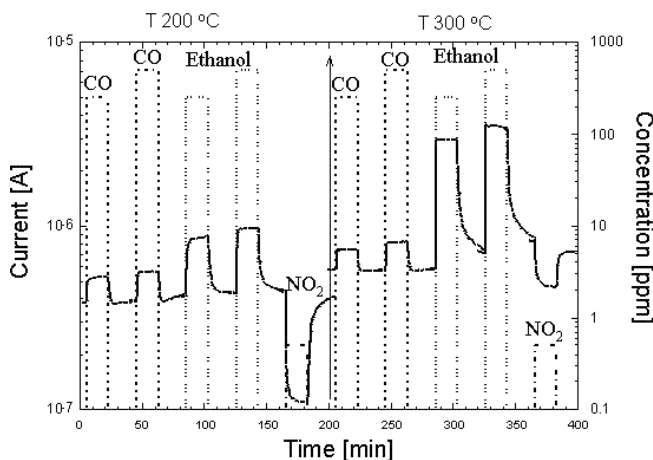


Fig. 6. Response of SnO<sub>2</sub> sensors to CO, ethanol, and NO<sub>2</sub> gases at  $200^\circ\text{C}$  and  $300^\circ\text{C}$ , at different gas concentrations. The left y-axis is for the change in electric current, and the right y-axis shows the gas concentration in parts per million.

## 7. Summary

Functional oxide nanobelts are a group of materials that have unique ribbon morphology. The nanobelts are single crystalline and free from dislocation, and their surfaces are atomically flat. The oxides are semiconductors, which can be used for the fabrication of nanoscale functional devices, such as field effect transistors and gas sensors. In contrast to carbon nanotubes whose semiconducting properties depend on the helical angle of the graphitic wall, the oxide nanobelts are semiconductive with a well-defined band structure and properties. The nanobelts and relevant nanostructures will have important applications in nanotechnology as nanoscale electronic, optical, sensor, and optoelectronic devices.

### Note added in proof:

After the submission of the manuscript, the following research has been carried out. The bending modulus of the ZnO nanobelt has been measured to be  $\sim 50$  GPa and the dual-mode resonance of a nanobelt has been observed.<sup>[25]</sup> The hardness of the nanobelts has been measured by a nano-indenter.<sup>[26]</sup> Thermal conductance across a single SnO<sub>2</sub> nanobelt has also been measured.<sup>[27]</sup> ZnO nanobelts have been manipulated and cut by an atomic force microscopy (AFM) tip for applications in microelectromechanical systems (MEMS) technology, and the re-shaped nanobelts have been demonstrated as nanoresonators and nanocantilevers<sup>[28]</sup>—50–1000 times smaller in width and length than conventional cantilevers. The nano-cantilever is expected to have much improved sensitivity and greatly improved mechanical flexibility for applications in scanning probe microscopy and sensor technology. Two volumes of books on nanowires and nanobelts have also been completed and are in press.<sup>[29,30]</sup>

- [1] Z. L. Wang, Z. C. Kang, *Functional and Smart Materials—Structural Evolution and Structure Analysis*, Plenum Press, New York **1998**.
- [2] Z. W. Pan, Z. R. Dai, Z. L. Wang, *Science* **2001**, 291, 1947.
- [3] Z. R. Dai, J. L. Gole, J. D. Stout, Z. L. Wang, *J. Phys. Chem. B* **2001**, 106, 1274.
- [4] M. H. Huang, S. Mao, H. Feick, H. Q. Yan, Y. Y. Wu, H. Kind, E. Weber, R. Russo, P. D. Yang, *Science* **2001**, 292, 1897.
- [5] M. H. Huang, Y. Y. Wu, H. Feick, N. Tran, E. Weber, P. D. Yang, *Adv. Mater.* **2001**, 13, 113.
- [6] Y. C. Kong, D. P. Yu, B. Zhang, W. Fang, S. Q. Feng, *Appl. Phys. Lett.* **2001**, 78, 407.
- [7] C. H. Liang, G. W. Meng, Y. Lei, F. Philipp, L. D. Zhang, *Adv. Mater.* **2001**, 13, 1330.
- [8] Y. Q. Zhu, W. K. Hsu, M. Terrones, N. Grobert, H. Terrones, J. P. Hare, H. W. Kroto, D. R. M. Walton, *J. Mater. Chem.* **1998**, 8, 1859.
- [9] X. C. Wu, W. H. Song, K. Y. Wang, T. Hu, B. Zhao, Y. P. Sun, J. J. Du, *Chem. Phys. Lett.* **2001**, 336, 53.
- [10] Z. L. Wang, R. P. Gao, J. L. Gole, J. D. Stout, *Adv. Mater.* **2000**, 12, 1938.
- [11] X. C. Wu, W. H. Song, W. D. Huang, M. H. Pu, B. Zhao, Y. P. Sun, J. J. Du, *Chem. Phys. Lett.* **2000**, 328, 5.
- [12] H. Z. Zhang, Y. C. Kong, Y. Z. Wang, X. Du, Z. G. Bai, J. J. Wang, D. P. Yu, Y. Ding, Q. L. Hang, S. Q. Feng, *Solid State Commun.* **1999**, 109, 677.
- [13] C. H. Liang, G. W. Meng, G. Z. Wang, Y. W. Wang, L. D. Zhang, S. Y. Zhang, *Appl. Phys. Lett.* **2001**, 78, 3202.
- [14] Z. G. Bai, D. P. Yu, H. Z. Zhang, Y. Ding, Y. P. Wang, X. Z. Gai, Q. L. Hang, G. C. Xiong, S. Q. Feng, *Chem. Phys. Lett.* **1999**, 303, 311.
- [15] Z. R. Dai, Z. W. Pan, Z. L. Wang, *Solid State Commun.* **2001**, 118, 351.
- [16] Z. W. Pan, Z. R. Dai, Z. L. Wang, *Appl. Phys. Lett.* **2002**, 80, 309.
- [17] P. D. Yang, C. M. Lieber, *Science* **1996**, 273, 1836.
- [18] R. S. Wagner, W. C. Ellis, *Appl. Phys. Lett.* **1964**, 4, 89.
- [19] Z. L. Wang, Z. W. Pan, *Adv. Mater.* **2002**, 14, 1029.
- [20] Z. R. Dai, Z. W. Pan, Z. L. Wang, *J. Am. Chem. Soc.* **2002**, 124, 8673.
- [21] Z. W. Pan, Z. R. Dai, C. Ma, Z. L. Wang, *J. Am. Chem. Soc.* **2002**, 124, 1817.
- [22] J. P. Schaffer, A. Saxena, S. D. Antolovich, T. H. Sanders, Jr., S. B. Warner, *The Science and Design of Engineering Materials*, 2nd ed., McGraw-Hill, New York **1999**, Ch. 6.
- [23] M. S. Arnold, P. Avouris, Z. W. Pan, Z. L. Wang, *J. Phys. Chem. B* **2003**, 107, 6.
- [24] E. Comini, G. Faglia, G. Sberveglieri, Z. W. Pan, Z. L. Wang, *Appl. Phys. Lett.* **2002**, 81, 1869.
- [25] X. D. Bai, E. G. Wang, P. X. Gao, Z. L. Wang, **2003**, unpublished.
- [26] S. Mao, M. Zhao, Z. L. Wang, **2002**, unpublished.
- [27] L. Shi, Z. L. Wang, unpublished.
- [28] W. Hughes, Z. L. Wang, **2003**, unpublished.
- [29] *Nanowires and Nanobelts of Functional Materials* (Ed: Z. L. Wang), Kluwer, Dordrecht, The Netherlands **2003**.
- [30] *Metal and Semiconductor Nanowires* (Ed: Z. L. Wang), Kluwer, Dordrecht, The Netherlands **2003**.